

Application of the multi-resolution viscous alignment technique to hourly radar rainfall estimation

Sudajai Lowanichchai^a, Uruya Weesakul^a, Virat Chatdarong^b, Siriluk Chumchean^{c,*}

^a Department of Civil Engineering, Thammasat University, Pathumthani 12121, Thailand

^b Department of Civil Engineering, Chulalongkorn University, Bangkok 10330, Thailand

^c Department of Civil Engineering, Mahanakorn University of Technology, Bangkok 10530, Thailand

*Corresponding author, e-mail: siriluk@mut.ac.th

Received 19 Jan 2009

Accepted 10 Jul 2009

ABSTRACT: The main objective of this paper is to improve the accuracy of radar rainfall estimation by accounting for a storm movement into a radar rainfall accumulation process. The multi-resolution viscous alignment (MVA) technique was used to estimate the velocity of a rain field from two consecutively measured radar images. The analysis used the 10-min radar reflectivity of the Pasicharoen radar and the corresponding 47 rain gauges measurements of 41 rainfall events that occurred in Bangkok during 2005–2007. The 28 rainfall events occurring during 2005–2006 were used for calibration, and the 13 rainfall events recorded in 2007 were used for validation. Finer temporal resolutions of radar reflectivity data, taken at 1–9 min intervals, were generated using the MVA technique in order to investigate the optimal temporal resolution of the Pasicharoen radar when the MVA technique was integrated into an hourly radar rainfall estimation algorithm to account for a storm movement within a sampling interval. The results showed that using the generated 5-min MVA reflectivity data for estimating hourly radar rainfall gave the smallest root mean square error (RMSE) between hourly radar rainfall estimates and corresponding rain gauge data when compared to other temporal resolutions of generated MVA reflectivity. Hourly radar rainfall obtained from the proposed algorithm, which integrates the MVA technique into the accumulation approach, was compared with the traditional simple linear interpolation (SLI) technique and conventional method. Using the 5-min generated MVA reflectivity data to estimate hourly radar rainfall can reduce RMSEs between hourly radar and rain gauge rainfall by 10% and 17% for the calibration period, and by 27% and 29% for the validation period when compared to the SLI and conventional methods, respectively.

KEYWORDS: effect of storm movement, storm tracking, radar rainfall accumulation

INTRODUCTION

The space-time resolution requirements for areal rainfall estimations vary depending on the application, catchment area, type of rainfall event, and type of model used¹. Accurate hourly areal rainfall with fine temporal resolution is an essential prerequisite for successful flood estimation and forecasts. Weather radar covering a large area provides spatially and temporally continuous measurements that can be used almost simultaneously as the storm occurs. However, radar rainfall measurement suffers from various types of errors and uncertainties^{2–5}. Methods to improve the accuracy of radar rainfall estimates have been proposed by many researchers. These include the algorithm to remove errors due to reflectivity measurement^{6–8}, $Z-R$ conversion error^{9–12}, and residual error in radar rainfall estimation when compared to rain gauge data^{13–15}. Radar usually operates a scheduler with volume scan by rotating the antenna in azimuth

while tilting the antenna vertically so as to sample the atmosphere as a series of cones. The rate at which a radar rotates about its axis, and the number of elevation angles used in one volume scan cycle fix the time between successive scans of the same position in space by the radar. This time difference represents the temporal resolution of the radar¹⁶. Conventional radar rainfall accumulation algorithm is normally derived by multiplying instantaneous radar rainfall intensity fields by the measured time interval between samples and then accumulating into a required temporal resolution. Consequently, there is an error in the derived areal radar rainfall particularly for a fast-moving storm.

Rainfall events occurring in the Bangkok area usually arise from convective clouds¹⁷. This is because Bangkok is located in the central part of Thailand which is influenced by southwest monsoons, tropical cyclones, and depressions. Convective rainfall is produced by adiabatic (constant heat) cooling of

vertically rising columns of air which have high temporal and spatial variabilities. Flooding in Bangkok is a serious problem since it causes enormous economic losses and also environmental impacts. The Bangkok Municipal Administration (BMA) has called for a flood forecasting system integrating information from rain gauges, hydrometric stations, radar measurements, satellite measurements, and numerical weather prediction results. The Pasicharoen radar data have been used in this project for providing hourly radar rainfall measurement and forecasts over the Bangkok vicinity. This radar operates every 10 min, and most of the rainfall events that lead to flooding in Bangkok are convective storms. Hence, there will be errors in hourly radar rainfall estimates and, consequently, rainfall forecasts. This is because the movement and development of the rainfall field often occur at a shorter time scale than the sampling interval.

The objective of this paper is to propose an hourly radar rainfall estimation process that accounts for a storm movement within the sampling interval. The multi-resolution viscous alignment (MVA) technique¹⁸ was used to estimate the velocity of a reflectivity field between two consecutive measured radar images and provide finer temporal reflectivity data between the sampling intervals. Radar reflectivity data from the Pasicharoen radar located in Bangkok and corresponding rain gauges data were used in this analysis. To investigate the optimal temporal resolution of the generated reflectivity data of the Pasicharoen radar when the MVA technique was integrated into an hourly radar rainfall estimation algorithm, finer temporal resolution of radar reflectivity data taken at 1-min to 9-min intervals were produced. Thereafter, the RMSEs between rain gauge data and radar rainfall obtained from different data sets were compared.

Effect of storm movement on radar rainfall

Many studies have investigated the effect of sampling interval on the radar rainfall accumulation process. They found that the error on radar rainfall estimation increased with increased space resolution and time between samples^{19–21}. The temporal resolution of radar rainfall measurement of most operational meteorological radars is 5–10 min. To obtain radar rainfall data at a required temporal resolution, these instantaneous radar rainfall maps are simply added by neglecting the fact that the storm moved and evolved during the sampling period. This leads to error on derived accumulated radar rainfall, especially for the case of a fast-moving storm such as convective rainfall.

To reduce the sampling problem on radar rainfall estimation, different tracking techniques have been

proposed to derive information on the movement and development of rainfall. This information has been used to simulate the rainfall development system between two consecutive radar samples. Thereafter, the measured and simulated rainfall fields are added to obtain accumulated radar rainfall data at a specified temporal resolution.

The tracking techniques can be classified into three main groups. The first group is the cell centroid tracking technique^{22–25}. This technique must first identify a rainfall cell by considering an exceeded intensity threshold. Then, the centre position, shape, and size of each rain cell are calculated. The identified cells of consecutive radar data samples are compared to the previous sample. If the corresponding movement vector and rate of change in size of a considered rain cell are within the allowed limits, the history of rain cell development is taken into account. Although this concept is simple, it is difficult to simulate an automatic model to identify the rain cell boundary, especially for joined or split cells. Moreover, each centroid velocity vector is not easy to derive²⁶. All existing centroid-type techniques use the storm centroid displacement to forecast the storm motion. This may result in large errors if the shape or sizes of the storm change rapidly²⁷.

The second group is the cross-correlation tracking technique^{28–31}. This technique divides Cartesian radar data into equally-spaced grid cells. A movement vector of each grid cell is derived by finding positions of cells from the Cartesian data array of the previous and the next radar data samples which have the highest similarity. The strength of this technique is that it provides more accurate velocity and position information of reflectivity echoes²⁴. However, Ravela and Chatdarong¹⁸ suggest that there are several disadvantages of this method.

The third group is the variational technique³². The basic idea of the variational technique is to guess a trial function for the problem and then adjust the function until the velocity field of the trial function is minimized. In this technique, an arithmetic equation or function represents an event or pattern of observation and its constrained function must be defined. The variational technique can be performed by following a model such as optical flow model³³, feature calibration alignment³⁴, data assimilation by field alignment³⁵, and MVA¹⁸. Frequently, all of these models provide intensive details of velocity field more accurately than the cell-centroid tracking and cross-correlation methods³⁴. The MVA method was directly developed from the field alignment³⁴ and the algorithm was extended into a multi-resolution pro-

cedure¹⁸ which is used to find displacement vectors more quickly than those procedures mentioned above. This technique derives a vector field from two images continuously by following the image flow approach³⁶. The displacement fields produced by MVA are dense, the spatial consistency of the displacement vector field is implicit, and high-order and small scale deformations can be handled easily. Unlike an optical-flow algorithm, it can calculate the displacement vector field from mesoscale features as a result of large time-steps or rapid deformation. In addition, the MVA algorithm produces displacement fields quickly. Therefore, in this study, the effect of storm movement within the sampling interval was accounted for in an hourly radar rainfall estimation algorithm by using the MVA technique to derive the reflectivity field velocity from two consecutive measured radar images. Thereafter, new reflectivity images between each sampling interval were generated and the hourly radar rainfall was derived by adding up the subsequent rainfall intensities within an hour.

Multi-resolution viscous alignment

The MVA algorithm uses a Bayesian formulation to solve the motion estimation problem and imposes smoothness constraints to provide a consistent velocity field. It is a position adjustment technique^{35,37}. It iteratively solves for the position error problem by minimizing an adjustment function based on gradient and divergence terms. This algorithm is practical for data without well-defined features and more robust than the correlation-based approaches where the displacement is given by the maximum correlation between two patches of images within a searching distance^{38,39}. In addition, the MVA technique uses local constraints for relating displacements and represents the displacement as smooth flow fields. This could be useful when working on a large region of the atmosphere where characteristics and features vary.

The concept of field alignment is demonstrated in Fig. 1. A state vector on a discrete grid is moved by deforming its grid (r) by a displacement (q). The displacement field q is real-valued, so $X(r - q)$ must be evaluated by interpolation. This displacement q represents a warping of the underlying grid, which in effect is able to move structures in the image around.

To calculate the field alignment we use¹⁸

$$w_1 \nabla^2 q_i + w_2 \nabla (\nabla q_i) + [\nabla X|_p H^T R^{-1} (HX(p) - Y)]_i = 0, \quad (1)$$

where H is transformation matrix which is an identity matrix, X and Y are the intensity scalar fields of

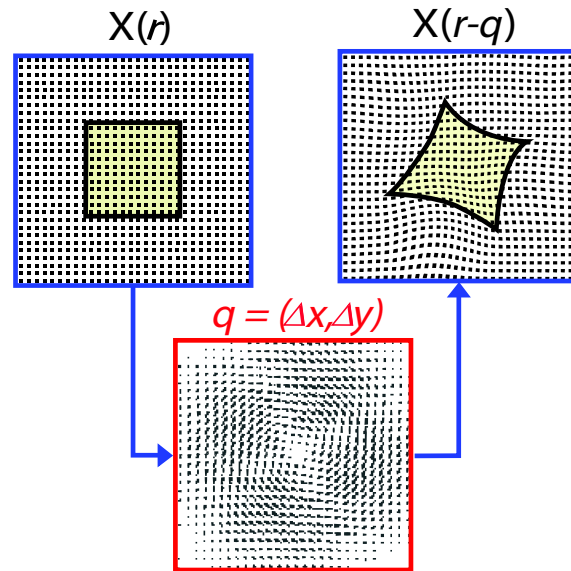


Fig. 1 Graphical illustration of field alignment. $X(r)$ is the image on the normal grid, q is a displacement vector, and $X(r - q)$ represents displacement of X by q . Δx and Δy are the difference in displacements in x and y directions, respectively.

the first and second images, respectively, R is the covariance matrix, q_i is the vector of displacements, and w_1 and w_2 are weight factors. Because the state of interest to be interpolated and the measurement are in dBZ units, the measurement is also performed at all pixels.

Eq. (1) is nonlinear and can be solved numerically by an iterative procedure similar to that used to solve the Poisson equation. An estimate of displacement can then be obtained. During each iteration, q_i is computed and used to deform the original image $X(r)$ to $X(r - q)$. The process is repeated using bi-cubic interpolation until the misfit between the deformation of the first image, $X(r - q)$, and the second image $Y(r)$ does not improve, or an iteration limit is reached. The vector of displacement q_i in (1) can be split into two velocity field equations; the velocity fields in x and y axes are $q_{xi} = \Delta x_i$ and $q_{yi} = \Delta y_i$, respectively. Finally, we have an aligned image, $X(r - q)$, with deformation and a displacement velocity field that is the sum of the displacement vector at each iteration $\hat{q} = \sum_{i=1}^N q_i$ for individual displacements \hat{q} at iterations $i = 1, \dots, N$. Since the process to obtain \hat{q} is time consuming, the multi-resolution concept is applied to speed up the algorithm. It starts by coarsening the resolution of the two images to obtain the coarse-scale displacement. At the coarser resolution, the alignment

will converge faster because the displacement will be small relative to the coarser resolution. Then, this coarse displacement velocity field is rescaled to the finer resolution and used to initially deform the finer resolution of X . Finally, the algorithm solves for another displacement field at the finer resolution and repeats the coarse-to-fine process until the resolution of interest is reached. When iteratively solving for (1), the unit of the displacement field \hat{q} is equal to the resolution of the underlying images X and $X(r - q)$. Therefore, it is essential to rescale the displacement field velocity when it is used at a different resolution, or when using the multi-resolution approach¹⁸.

DATA COLLECTION

Radar reflectivity data

The polar plan position indicator (PPI) reflectivity data of rainfall events recorded from the C-band Pasicharoen radar were used in the analysis. The Pasicharoen radar is located in the western part of Bangkok, and belongs to the BMA. The radar transmitted radiation with wavelength of 5.42 cm and produced a beam with a 40 dB width of 2.2° . It was operated in a volume scan mode by measuring reflectivity data from 3 elevation angles (0.5° , 1.5° , 3.5°) every 10 min. To avoid the effects of the bright band, the PPI reflectivity data used in this study were extracted from the raw polar data at the lowest elevation where the height of radar beam was below the freezing level of the study area. These polar data were converted to lie on a $120 \text{ km} \times 120 \text{ km}$ Cartesian grid with $0.5 \text{ km} \times 0.5 \text{ km}$ spatial resolution and 10 min temporal resolution. To avoid the effects of noise and hail, the measured radar reflectivity, values that were less than 15 dBZ were assumed to represent zero reflectivity of and the reflectivity values that were greater than 53 dBZ were assumed to be 53 dBZ⁴⁰. Additionally, the errors due to the effect of ground clutter were also removed from the reflectivity data by using a map of known ground clutter locations, and the radar measurement was discarded and interpolated in these areas. In this study, 41 rainfall events which occurred in Bangkok during June 2005 to September 2007 were used. (Table 1).

Gauge rainfall data

Rain gauge data used in this study were obtained from a network of 47 tipping bucket rain gauge stations located 5–50 km from the radar site (Fig. 2). These rain gauge stations are owned and operated by BMA. All of these stations have a tipping bucket size of 0.5 mm and record rainfall data every 15 min. Quality

Table 1 Rainfall events used in the analysis.

Start time	Duration (min)	Number of gauges	R_{avg} (mm/h)	R_{max} (mm/h)
18:20 23/06/05	120	28	11.14	132.00
17:20 29/06/05	130	26	11.35	84.00
16:10 03/07/05	60	10	8.19	52.80
08:20 10/07/05	200	34	29.44	98.00
16:20 28/07/05	70	23	6.56	63.80
16:51 12/10/05	90	9	18.39	77.00
02:41 14/10/05	280	33	17.58	105.60
14:01 14/10/05	150	11	11.03	105.60
19:41 15/10/05	120	17	5.71	46.20
15:31 19/10/05	230	37	24.7	94.60
17:01 26/10/05	170	20	8.65	85.40
17:01 04/11/05	80	12	12.14	103.40
11:31 08/11/05	170	20	19.32	114.20
13:21 11/11/05	120	14	24.35	99.00
12:31 12/11/05	110	10	9.78	90.20
16:11 18/11/05	100	23	9.28	73.20
11:31 20/02/06	70	21	18.54	52.80
14:51 01/07/06	390	43	6.37	15.40
17:01 02/07/06	180	39	5.70	23.10
20:01 30/08/06	270	32	7.44	17.05
21:51 07/09/06	200	29	8.01	32.27
11:31 26/09/06	130	13	2.92	16.50
15:31 26/09/06	260	32	12.39	28.05
19:11 27/09/09	130	20	5.61	24.20
11:11 05/10/06	200	15	3.31	28.05
00:41 10/10/06	170	21	4.05	14.70
00:01 18/10/06	150	27	4.52	20.35
12:21 18/10/06	220	12	5.44	22.00
06:01 19/03/07	100	17	1.20	59.46
03:11 20/03/07	150	26	15.73	79.47
11:01 09/05/07	140	25	34.26	85.33
09:31 10/05/07	230	27	7.88	100.93
16:41 14/05/07	160	37	14.84	68.40
15:01 16/06/07	350	46	24.20	115.06
17:01 20/07/07	250	28	5.28	64.00
11:21 23/07/07	150	29	8.39	106.66
11:51 25/07/07	260	37	28.64	121.60
19:31 10/09/07	110	41	18.86	64.80
18:11 11/09/07	90	44	15.80	83.60
00:01 19/09/07	180	37	17.97	54.13
20:21 20/09/07	80	38	11.44	45.06

Accumulated rain gauge rainfall were averaged from rainfall $> 0.5 \text{ mm/h}$;

R_{max} is the maximum rain gauge rainfall.

control of these data was performed by considering rainfall data from adjacent gauges and the plots of time series. If unusual rainfall data were found, these data were excluded from the analysis. Note that rain gauge stations less than 5 km from the radar site were not used as the radar could not provide reflectivity data

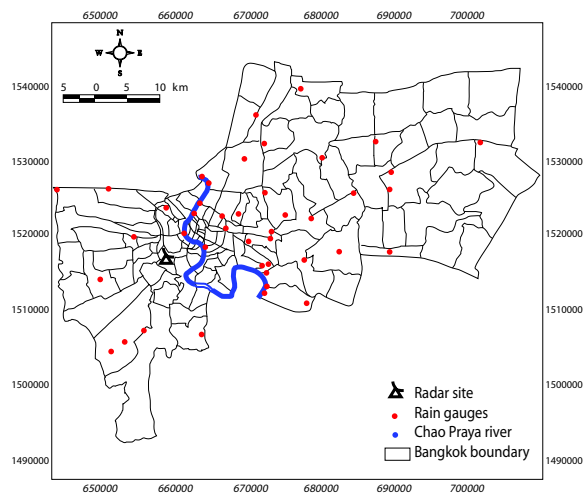


Fig. 2 Map of Bangkok area showing rain gauges (small circles) and the Pasicharoen radar (radar symbol).

for them.

METHOD

Application of MVA technique for temporal downscaling of reflectivity data

The MVA technique is applied to reflectivity fields, not rainfall rates, because the power law relationship between reflectivity and rainfall rate will have an effect on spatial interpolation that is used to generate intermediate data fields. The following procedures were followed to generate new radar images between two consecutive reflectivity measurements.

Step 1. Assign time interval t , $t_1 < t < t_2$ where t_1 and t_2 represent times of the first and the second images, respectively.

Step 2. For each time interval, the forward and backward weight factors are calculated from $w_1 = (t - t_1)/(t_2 - t_1)$ and $w_2 = (t_2 - t)/(t_2 - t_1)$, respectively.

Step 3. Read reflectivity from row and column data files to matrix. Let A = the first image, B = the second image, C = new generated image, and V = velocity.

Step 4. Produce new forwards and backwards images by using $C_{12} = w_1AV_1$ and $C_{21} = w_2BV_2$, respectively.

Step 5. Produce a new image using $C = w_2C_{12} + w_1C_{21}$.

Step 6. Repeat steps 1 to 5 by changing $t = 1, 2, 3, 4, 5, 6, 7, 8,$ and 9 min.

An example of a comparison between generated radar images based on MVA and simple linear in-

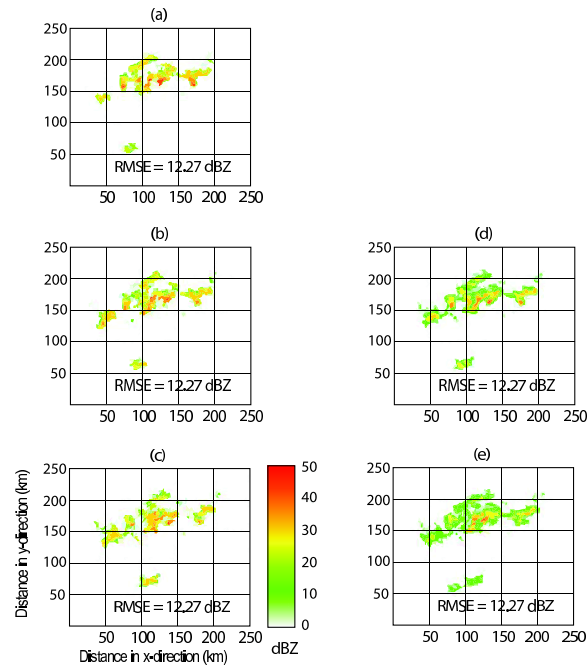


Fig. 3 Comparison between observed radar images measured on 26 September 2009 and generated radar images based on MVA and SLI methods: (a–c) Measured radar images at 17:21, 17:31, and 17:41, respectively. Generated images for 17:31 using (d) MVA estimation (e) SLI estimation.

terpolation (SLI) is illustrated in Fig. 3. The RMSEs of the generated reflectivity, image obtained by using the MVA and SLI methods were 12.72 dBZ and 13.25 dBZ, respectively, when compared to the observed reflectivity image. It is evident that the generated radar reflectivity image based on the MVA technique is closer to the observed reflectivity image than that generated based on the SLI method. It should be noted that the radar image generated from SLI method was calculated by using $w_2A + w_1B$.

Investigation of the optimum temporal resolution of generated reflectivity data

To investigate the optimum temporal resolution of generated reflectivity data when the MVA technique is integrated into radar rainfall estimation process, new reflectivity images between two consecutive measured reflectivity data were generated with different temporal resolutions. Since the 10-min reflectivity data were available in this study, MVA reflectivity data with 1-min to 9-min temporal resolutions were generated. The generated reflectivity data were divided into 9 data sets. The number of generated reflectivity images between two consecutive reflectivity measurements

were 8, 4, 3, and 1 for the 1-, 2-, 3-, and 4 to 9-min temporal resolutions, respectively. Note that the calculation time for generating one reflectivity image is about 42 s (based on core2DUO 1.8 GHz). The climatological MVA $Z-R$ parameters of the 9 data sets were calculated, and estimated radar rainfall obtained from the 9 data sets were compared. The optimum temporal resolution was examined by considering the smallest RMSE between rain gauge and radar rainfall of each data set. The RMSEs of the radar rainfall estimates at the rain gauge locations were used to evaluate the quality of radar rainfall. The RMSEs can be estimated from

$$\text{RMSE} = \sqrt{\frac{1}{N} \sum_{t=1}^{N_t} \sum_{i=1}^{N_G} (R_{i,t} - G_{i,t})^2},$$

where $R_{i,t}$ is the radar-rainfall accumulations at the pixel corresponding to the i th rain gauge for hour t , $G_{i,t}$ is the corresponding rain gauge rainfall for hour t , N_G is the number of rain gauges that measure nonzero rainfall, N_t is the number of time periods (in hours), and N is the total number of radar-gauge pairs used in the computation.

Calibration of climatological $Z-R$ relationship

Radar rainfall is derived by converting measured radar reflectivity (Z) into rainfall intensity (R) using an appropriate $Z-R$ relationship⁴¹ that can be expressed as $Z = aR^b$, where a and b are model parameters which depend on the rainfall drop size distributions that have been sampled, assuming that the terminal velocity of the raindrops is a function of their diameter, and that they are falling at terminal velocity through still air¹³. Parameters of climatological $Z-R$ relationship are usually calibrated using reflectivity and a rain gauge network data over a period. Estimation of the coefficients a and b in the $Z-R$ relation involves minimization of a measure of error between the estimated radar rainfall and corresponding rain-gauge data. Doelling et al⁴², Steiner and Smith⁴³ and Hagen and Yuter⁴⁴ studied parameters of the $Z-R$ relationship using several years of disdrometer data. They found that the most suitable value of b was 1.5. In the same way, the results from the study by Seed et al⁴⁵ showed that variation of b did not affect the RMSE between radar and rain gauge rainfall much. Therefore, in this study we used $b = 1.5$ and the value of a was estimated by minimizing the RMSE between rain gauge and radar-rainfall estimates.

To study the effectiveness of the MVA algorithm to radar rainfall estimation, three different climatological $Z-R$ relationships were estimated. Firstly, the $Z-$

R relationship was retrieved by calibration using the 10-min reflectivity data, hereafter referred as conventional calibrated $Z-R$. Secondly, the SLI technique was used to generate 5-min reflectivity data. These 5-min SLI generated reflectivity data were used for calibration of the SLI $Z-R$ relationship. Thirdly, the MVA algorithm presented in the earlier section was used for temporal downscaling of radar reflectivity in order to increase the frequency of the reflectivity data. The 5-min MVA reflectivity data were generated and used for calibrating the MVA $Z-R$ relationship. The calibrations of the above three cases were performed hourly. The reflectivity data settings of the three cases and the corresponding rain gauge rainfall of 28 rainfall events that occurred from June 2005 to October 2006 were used for calibration of the three $Z-R$ relationships. These three derived relationships were used for converting their corresponding reflectivity data sets into rainfall intensities. Then an accumulation algorithm was used to accumulate radar rainfall intensities into an hourly time-step. In addition, the uncalibrated $Z-R$ relationship ($Z = 200R^{1.6}$)⁴¹ was also used to convert the three reflectivity data settings into rain rates for comparison.

To confirm the utility of the estimated $Z-R$ parameters obtained from the three cases, a validation was performed using 13 rainfall events that occurred during 2007. The effectiveness of applying the MVA technique to radar rainfall estimation was evaluated by comparing RMSEs between hourly rainfall and hourly radar rainfall obtained from the above cases.

RESULTS

Optimum temporal resolution of generated MVA reflectivity data

Nine finer temporal resolutions (1 min to 9 min) of radar reflectivity data settings of the 28 calibrated rainfall events were generated using the MVA technique as explained in the previous section. The a parameters of the MVA $Z-R$ relationships of these 9 data sets are presented in Fig. 4(a). It should be noted that high variability in a for the calibrated $Z-R$ relationships illustrates that these parameters were sensitive to the reflectivity data settings used for the calibration. Since this paper aims to investigate the effectiveness of applying of the MVA technique to hourly radar rainfall estimation, variability of the a values obtained from different data settings should not affect the result of this study because they have been applied to their corresponding data sets. These derived MVA $Z-R$ relationships were used to estimate the corresponding radar rainfall intensity. Then, the hourly radar rainfall

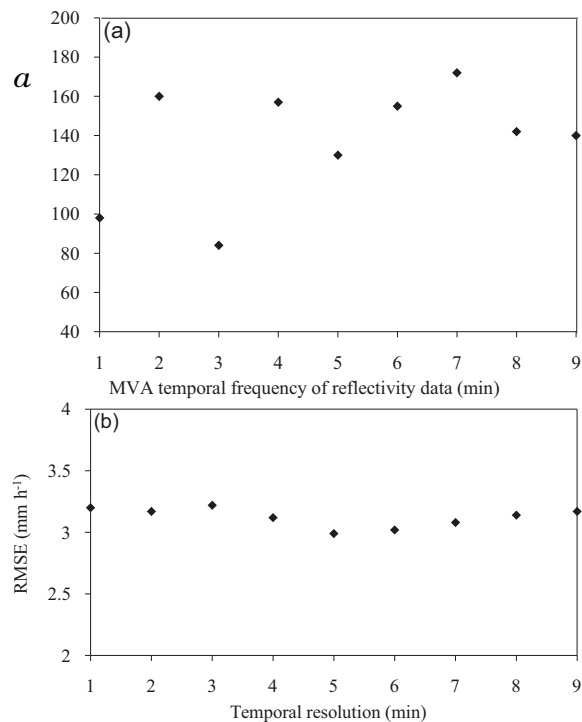


Fig. 4 (a) Variation of α of the calibrated MVA $Z-R$ relationships; (b) RMSE between radar rainfall estimates from different frequencies of MVA reflectivity data and rain gauge measurement.

was obtained by adding up the subsequent rainfall intensity within an hour. The RMSEs between hourly radar rainfall and the corresponding rain gauge data of these 9 data sets were calculated and plotted as illustrated in Fig. 4(b). The results showed that the 5-min temporal resolution of generated MVA reflectivity data gave the smallest RMSE. Moreover, the computation time used to generate 5-min temporal resolution of MVA reflectivity data was less than the temporal resolutions at 1- to 4-min and it was equal to the 6-, 7-, 8- and 9-min temporal resolutions. Based on the data used in this study, we can consider that the optimum temporal resolution of the generated reflectivity data using the MVA technique is 5 min.

Effectiveness of applying MVA technique into hourly radar rainfall estimates Calibration result

Three reflectivity data settings, i.e., measured 10-min reflectivity, 5-min SLI reflectivity, and 5-min MVA reflectivity of the ensemble of 28 rainfall events which occurred during June 2005 to October 2006 were used to calibrate the climatological $Z-R$ (conventional calibrated $Z-R$), climatological 5-min SLI $Z-R$ and climatological 5-min MVA $Z-R$ relationships,

Table 2 Climatological $Z-R$ relationships of the ensemble of 28 calibrated events.

Reflectivity data settings	$Z-R$ relationship	RMSE* (mm/h)
Measured 10-min reflectivity	$Z = 200R^{1.6}$	3.66
5-min SLI reflectivity	$Z = 45R^{1.5}$ (calibrated)	3.61
5-min MVA reflectivity	$Z = 200R^{1.6}$	3.45
	$Z = 86R^{1.5}$ (calibrated)	3.32
	$Z = 200R^{1.6}$	3.29
	$Z = 130R^{1.5}$ (calibrated)	2.99

* RMSE between hourly radar rainfall estimates and corresponding rain gauge data.

respectively. The calibrations were performed at hourly time steps and the results are present in Table 2. It was found that the climatological conventional calibrated $Z-R$, climatological calibrated 5-min SLI $Z-R$, and climatological calibrated 5-min MVA $Z-R$ relationships were $Z = 45R^{1.5}$, $Z = 86R^{1.5}$, and $Z = 130R^{1.5}$, respectively. Hourly radar rainfall of the above three data settings was estimated using their corresponding $Z-R$ relationships. RMSEs between rain gauge data and hourly radar rainfall of the ensemble of the 28 events that were calculated by using the three reflectivity data sets and their corresponding calibrated $Z-R$ relationships were 3.61 mm/h, 3.32 mm/h, and 2.99 mm/h, respectively. Based on the 28 calibrated rainfall events, we found that applying the MVA technique to hourly radar rainfall estimation could reduce RMSEs between hourly radar rainfall and rain gauge data when compared to the calibrated 5-min SLI $Z-R$ and conventional methods. The improvement in the accuracy of radar rainfall was the result of accounting for the effect of storm movement within the sampling interval into radar rainfall accumulation by increasing reflectivity data between two consecutive reflectivity images using the MVA technique. Nevertheless, a validation process needs to be performed to confirm the effectiveness of applying the MVA technique into radar rainfall estimation. Different rainfall events that had not been used in the calibration process were used for validation purposes.

Validation result

The validation was performed to confirm whether the calibration results presented earlier hold true in a generic situation. The assessment was performed based on the rainfall events that were not used for estimating the $Z-R$ relationship, and hence provide a good indication of how either approach performs.

Table 3 RMSEs between radar rainfall estimates and rain gauge data of the validation events.

Event	RMSE (mm/h)					
	Measured 10-min reflectivity		5-min SLI reflectivity		5-min MVA reflectivity	
<i>a</i>	200	45	200	86	200	130
<i>b</i>	1.6	1.5	1.6	1.5	1.6	1.5
19 Mar	2.36	2.19	2.29	2.13	2.09	0.59
20 Mar	4.54	3.54	4.03	3.42	3.99	2.39
9 May	4.36	3.96	3.97	3.87	4.17	3.37
10 May	3.89	3.75	3.43	3.25	3.19	1.96
14 May	4.32	3.52	4.25	3.15	2.84	2.97
16 May	5.12	4.84	5.08	4.80	4.78	4.80
20 July	4.24	4.11	4.36	3.94	5.26	1.10
23 July	3.88	3.64	3.76	3.17	3.78	1.85
25 July	5.28	5.01	5.52	5.33	6.3	5.07
10 Sep	3.43	3.03	3.18	3.01	2.97	2.84
11 Sep	3.89	3.49	3.79	3.26	3.66	2.24
17 Sep	4.23	3.26	4.19	3.34	4.17	2.88
20 Sep	3.94	3.24	3.73	3.56	2.04	1.88
Mean	4.11	3.66	3.96	3.56	3.79	2.61

13 rainfall events which occurred during March–September 2007 were used for validation. These rainfall events had not been used for calibration. Accuracies of radar rainfall estimates were compared for six different cases (Table 3).

From Table 3, we found that accounting for storm movement by applying MVA technique to increase temporal frequency of reflectivity data (rightmost column in Table 3) gave the smallest RMSEs for all of the validation rainfall events. The validation results showed that, on average, integrating the MVA technique into the hourly radar rainfall estimation process could reduce RMSEs between hourly radar rainfall and rain gauge measurement by 0.95 mm/h and 1.05 mm/h when compared to using the SLI and conventional methods, respectively. This confirmed the effectiveness of the MVA Z – R relationship and the efficiency of the MVA technique for taking into account the effect of storm movement on hourly radar rainfall estimates.

CONCLUSIONS

The main conclusions of this study are as follows. (1) The optimum temporal resolution of generated reflectivity data of the Pasicharoen radar based on the MVA technique is 5 min. (2) The climatological Z – R relationship of the Pasicharoen radar based on 5-min MVA reflectivity data is $Z = 130R^{1.5}$. (3) Accounting for the storm movement in hourly radar rainfall es-

timation by using the MVA technique to calculate the velocity of reflectivity field and generating reflectivity data between two consecutive measured radar images can reduce RMSEs between hourly radar and rain gauge rainfall by 0.33 mm/h and 0.62 mm/h for the calibration period and by 0.95 mm/h and 1.05 mm/h for the validation period when compared to the SLI and conventional methods, respectively.

Acknowledgements: The authors gratefully acknowledge the Department of Drainage and Sewerage of the Bangkok Municipal Administration for providing the radar and rain gauge data.

REFERENCES

- Cole J, Moore J (2008) Hydrological modeling using raingauge- and radar-based estimations of areal rainfall. *J Hydrol* **358**, 159–81.
- Fabry F, Bellon A, Duncan MR, Austin GL (1994) High resolution rainfall measurement by radar for very small basin: The sampling problem re-examined. *J Hydrol* **116**, 415–28.
- Jordan PW, Seed AW, Austin GL (2000) Sampling errors in radar estimates of rainfall. *J Geophys Res* **105**, 2247–57.
- Krajewski WF, Smith JA (2002) Radar hydrology: rainfall estimation. *Adv Water Resour* **25**, 1387–94.
- Chumchuan S, Sharma A, Seed A (2006) An integrated approach to error correction for real-time radar-rainfall estimation. *J Atmos Ocean Tech* **23**, 67–79.
- Anagnatsou EN, Morales CA (2001) Rainfall estimation from TOGA radar observations during the LBA field campaign. *J Geophys Res* **107**, 66–91.
- Chumchuan S, Sharma A, Seed A (2004) Application of scaling in radar reflectivity for correcting range-dependent bias in climatological radar rainfall estimates. *J Atmos Ocean Tech* **21**, 1545–56.
- Öztürk K, Yilmazer AU (2007) Improving the accuracy of the radar rainfall estimates using gage adjustment techniques: Case study for West Anatolia, Turkey. *Atmos Res* **86**, 139–48.
- Joss J, Waldvogel A (1990) Precipitation measurement and hydrology. In: Atlas D (ed) *Radar in Meteorology: Battan Memorial and 40th Anniversary Radar Meteorology*, Amer Meteor Soc, Boston, pp 577–606.
- Liu C (1995) Numerical analysis of error quantification and propagation in radar remote sensing for rainfall estimation. PhD thesis, Univ of Iowa.
- Collier CG (1996) *Applications of Weather Radar Systems: A Gauge to Uses of Radar in Meteorology and Hydrology*, Wiley, New York.
- Chumchuan S, Sharma A, Seed A (2008) An operational approach for classifying storms in real-time radar rainfall estimation. *J Hydrol* **363**, 1–17.
- Chumchuan S, Sharma A, Seed A (2006) Correcting

- of real-time radar rainfall bias using a Kalman filtering approach. *J Hydrol* **317**, 123–37.
14. Ciach GJ, Krajewski WF, Villarini G (2007) Product-error-driven uncertainty model for probabilistic precipitation estimation with NEXRAD data. *J Hydrometeorol* **8**, 1325–47.
 15. Germann U, Berenguer M, Sempere-Torres D, Zappa M (2009) REAL - Ensemble radar precipitation estimation for hydrology in a mountainous region. *Q J Roy Meteorol Soc* **135**, 445–56.
 16. Smith JA, Krajewski WF (1991) Estimation of mean field bias of radar rainfall estimates. *J Appl Meteorol* **30**, 397–412.
 17. Talumassawatdi R (2006) Radar rainfall estimates. Technical Notes, Royal Rainmaking and Agricultural Aviation, April 2006, Bangkok.
 18. Ravela S, Chatdarong V (2006) Rainfall advection using velocimetry by multiresolution viscous alignment. arXiv:physics/0604158.
 19. Harrold TW, English EL, Nicholass CA (1974) The accuracy of radar-derived rainfall measurements in hilly terrain. *Q J Roy Meteorol Soc* **100**, 331–50.
 20. Wilson JW, Brandes EA (1979) Radar measurement of rainfall—a summary. *Bull Am Meteorol Soc* **60**, 1048–58.
 21. Anagnostou EN, Krajewski WF, Smith JA (1999) Uncertainty quantification of mean areal radar-rainfall estimates. *J Atmos Ocean Tech* **16**, 206–15.
 22. Rosenfeld D (1987) Objective method for analysis and tracking of convective cells as seen by radar. *J Atmos Ocean Tech* **4**, 422–34.
 23. Dixon M, Weiner G (1993) TITAN: Thunderstorm identification, tracking, analysis and nowcasting – A radar based methodology. *J Atmos Ocean Tech* **10**, 785–97.
 24. Johnson JT, MacKeen PL, Witt A, Mitchell ED, Stumpf GJ, Eilts MD, Thomas KW (1998) The Storm Cell Identification and Tracking (SCIT) algorithm: An enhanced WSR-88D algorithm. *Weather Forecast* **13**, 263–76.
 25. Handwerker J (2002) Cell tracking with TRACE3D—a new algorithm. *Atmos Res* **61**, 15–34.
 26. Hannesen R (2002) An enhanced surface rainfall algorithm for radar data. Deliverable 4.4, Multiple-Sensor Precipitation Measurements, Integration, Calibration and Flood Forecasting (MUSIC).
 27. Han L, Fu S, Yang G, Wang H, Zheng Y, Lin Y (2008) A stochastic method for convective storm identification, tracking and nowcasting. *Progr Nat Sci* **18**, 1557–63.
 28. Hilst GR, Russo JA Jr (1960) An objective extrapolation technique for semiconservative fields with an application to radar patterns. Tech Memo No 3, Travelers Weather Research Center, Hartford, CT.
 29. Rinehart RE, Gravy ET (1978) Three-dimension storm motion detect by conventional weather radar. *Nature* **273**, 287–9.
 30. Tuttle JD, Foote GB (1990) Determination of the boundary layer airflow from a single Doppler radar. *J Atmos Ocean Tech* **7**, 218–32.
 31. Li L, Schmid W, Joss J (1995) Nowcasting of motion and growth of precipitation with radar over a complex orography. *J Appl Meteorol* **34**, 1286–300.
 32. Euler L (1744) *Methodus Inveniendi Lineas Curvas Maximi Minimive Proprietate Gaudentes* (A method for finding curves processing maximal and minimal properties), Lausanne and Geneva, Springer-Verlag, New York.
 33. Bowler NE, Pierce CE, Seed A (2004) Development of a precipitation nowcasting algorithm based upon optical flow techniques. *J Hydrol* **288**, 74–91.
 34. Chatdarong V (2006) Multi-sensor rainfall data assimilation using ensemble approaches. PhD thesis, MIT.
 35. Ravela S, Emanuel SK, McLaughlin D (2006) Data Assimilation by Field Alignment. *Physica D* **230**, 127–45.
 36. Subbarao M (1989) Interpretation of image flow: a spatio-temporal approach. *IEEE Trans Pattern Anal Mach Intell* **11**, 266–78.
 37. Ravela S (2006) Amplitude-position formulation of data assimilation. In: *Computational Science - ICCS 2006, Proceedings Part III*, Springer-Verlag, Berlin, pp 497–505.
 38. Junck L, Moen JG, Hutchins GD, Brown MB, Kuhl DE (1990) Correlation methods for the centering, rotation, and alignment of functional brain images. *J Nucl Med* **31**, 1220–6.
 39. Dong L, Boyer AL (1996) A portal image alignment and patient setup verification procedure using moments and correlation technique. *Phys Med Biol* **41**, 697–723.
 40. Fulton RA, Breidenbach JP, Seo D-J, Miller DA, Brannon TO (1998) The WSR-88D rainfall algorithm. *Weather Forecast* **13**, 377–95.
 41. Marshall JS, Palmer WM (1948) The distribution of raindrops with size. *J Meteorol* **5**, 165–6.
 42. Doelling IG, Joss J, Riedel J (1998) Systematic variations of $Z - R$ -relationships from drop size distributions measured in northern Germany during seven years. *Atmos Res* **47–48**, 635–49.
 43. Steiner M, Smith JA (2000) Reflectivity, rain rate, and kinetic energy flux relationships based on raindrop spectra. *J Appl Meteorol* **39**, 1923–40.
 44. Hagen M, Yuter SE (2003) Relations between radar reflectivity, liquid water content, and rainfall rate during the MAP-SOP. *Q J Roy Meteorol Soc* **128**, 477–93.
 45. Seed A, Siriwardena L, Sun X, Jordan P, Elliott J (2002) On the calibration of Australian weather radars, Tech Rep 02/7 Cooperative Research Centre for Catchment Hydrology, Melbourne, p 40.